

Zr-2.5%Nb**The effects of directional deformation behavior
on DHC behavior in Zr-2.5%Nb pressure tube**

* , , ,

150

Zr-2.5%Nb

DHC

DHC

가

100-400°C

가

. DHC

DHC

가

CT CB

DHC

Abstract

To explain the anisotropy of delayed hydride cracking (DHC) behavior in the longitudinal and radial directions in Zr-2.5%Nb pressure tube materials, tensile behavior in the radial direction and the texture change in the DHC surfaces have been examined. The deformation behavior in the radial direction appeared similar to that of transverse direction and the yield strength in the radial direction is minimum in the range of 100-400°C. It has been found that plastic deformation occurs during DHC process and the deformation mechanisms operating during the cracking process were clearly different in both specimens. Therefore, it can be concluded that the differences in crack propagation behavior between CT and CB specimens are due to the differences in deformation mechanisms.

1.

Zr-2.5%Nb

DHC

가 CT

CB

DHC

[1, 2].

DHCV

DHCV

2

Fig. 1

DHC

(K_{IH})

K_{IH} 가 50%

Fig. 2[2-7]

CT CB

CT

, CB

DHC

Zr-2.5%Nb

K_{IH}

가

[3].

(F)

(1-F)

가

$$K_{IH} = K_{IC \text{ of ductile matrix}} \times (1-F) + K_{IC \text{ of brittle hydride}} \times F \quad (1)$$

K_{IH} 가

가

Coleman

[8].

DHC

가

DHC

XRD

DHC

2.

DHC 가 60ppm CT CB ,
Fig. 3 . CT 가
creep , CB (AE, acoustic
emission) computer
controlled tester .

DHC XRD
, DHC .

(inverse pole figure) .

Fig. 4 gage
section 가 2mm ,

가 (electric discharge machining, EDM) , EDM 가
0.1mm 560°C ,
5x10⁻⁴/s .

3.

Zr-2.5%Nb CANDU Fig. 5 . HCP
á-Zr c , prism
plane [10.1] . Fig.
5 , , 가

DHC CB CT Fig.
10% 20% ,
6 Fig. 7 .

XRD
가 가 .
가

Fig. 6 c) Fig. 7 c) CT
 CB (11 $\bar{2}$ 1) (10 $\bar{1}$ 2) 가
 CT CB DHC 가
 CT (10 $\bar{1}$ 2) Fig. 5 b) c) 가
 Schmid factor가 (10 $\bar{1}$ 2) 가
 , CB Fig. 5 a) b) (11 $\bar{2}$ 1) c) 가
 (10 $\bar{1}$ 2) Schmid factor가 가
 30° (11 $\bar{2}$ 1) Schmid factor가 가
 , 가 (10 $\bar{1}$ 2) Schmid factor가
 Fig. 8, 9 , ,
 150 가 가 400
 가 100-400°C Fig. 10 11 가 ,
 가 가
 가 가
 가 , 2) CT CB 가
 가 , 3) , 가

가 DHC

DHC

Fig. 5 a)

가 , DHC

, 가

CB

DHC

가

CT

DHC

Fig. 12 three point bend

j-integral

250°C

60 ppm

60 ppm

250°C

60 ppm

250°C

three point bend

가

DHC

CT

CB

DHC

가

4.

1) Zr-2.5%Nb

DHC

$(10\bar{1}2)$

, CB

CT

$(11\bar{2}1)$ $(10\bar{1}2)$

2)

DHC

References

1. S. Sagat, C. E. Coleman, M. Griffiths, and B. J. S. Wilkins, Zirconium in the Nuclear Industry, Tenth International Symposium, ASTM STP 1245, 1994, pp. 35-61.
2. S. S. Kim, S. C. Kwon, K. N. Choo, Y. M. Cheong, and Y. S. Kim, Key Engineering Materials, Vols 183-187 (2000), PP. 845-850.
3. S. S. Kim, S. C. Kwon, and Y. S. Kim, J. Nucl. Mater. Vol. 273, 1999, pp.52-59.
4. C. E. Coleman, S. Sagat, and K. F. Amouzouvi, Control of Microstructure to Increase the Tolerance of Zirconium Alloys to Hydride Cracking, Atomic Energy of Canada Limited Report AECL-9524 (1987).
5. C. E. Coleman, Zirconium in the Nuclear Industry, Fifth Conference, ASTM STP 754, 1982, pp. 393-411.
6. H. Huang, and W. J. Mills, Metal. Transactions A 22A (1991), pp.2149-2060.
7. W. J. Mills, and F. H. Huang, Eng. Frac. Mech. 39 (1991), pp. 241-257.
8. C. E. Coleman, B. A. Cheadle, C. D. Cann, and J. R. Theaker, Zirconium in the Nuclear Industry, Eleventh International Symposium, ASTM STP 1295, 1996, pp. 884-898.

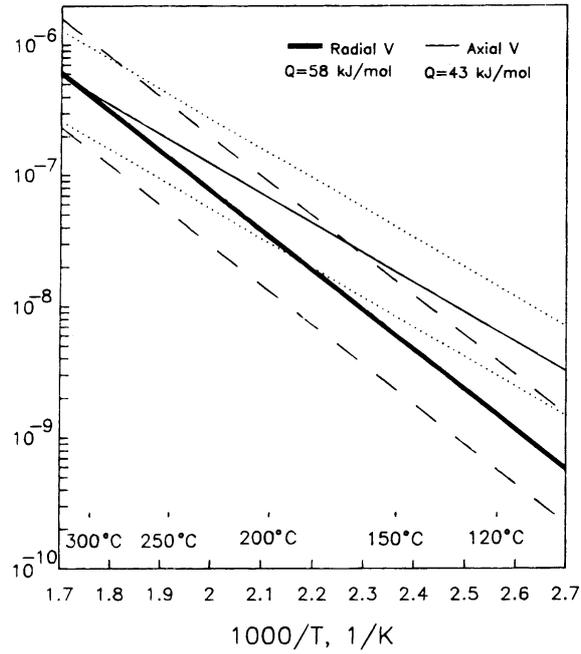


Fig. 1. Comparison of DHC velocity in the radial and longitudinal direction [1].

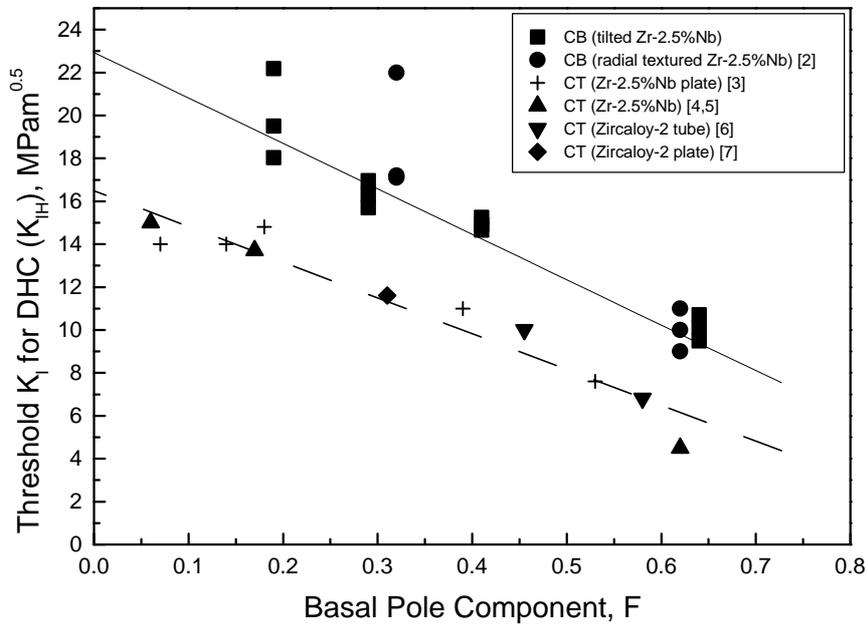
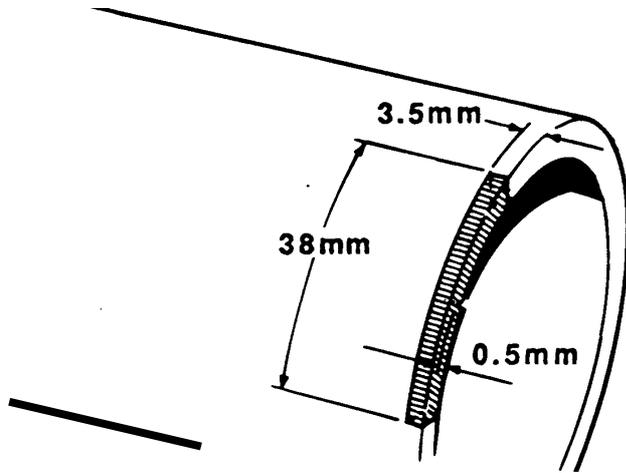


Fig. 2. Comparisons of K_{IH} measured from CT and CB specimens with the basal pole components in Zircaloy-2 and Zr-2.5%Nb materials [2-7].

a) cantilever beam specimen



b) curved compact tension specimen

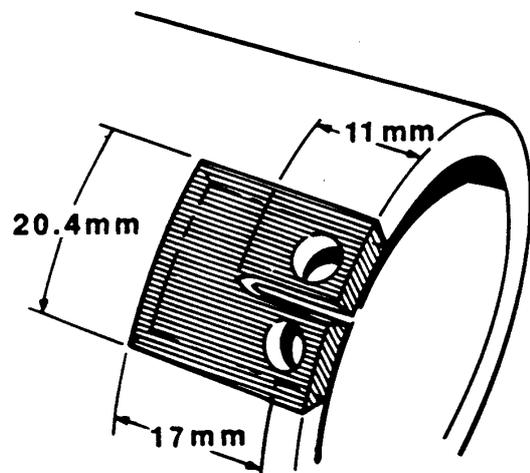


Fig. 3. Schematic illustration of a) cantilever beam (CB) and b) curved compact tension (CCT) specimens [1].

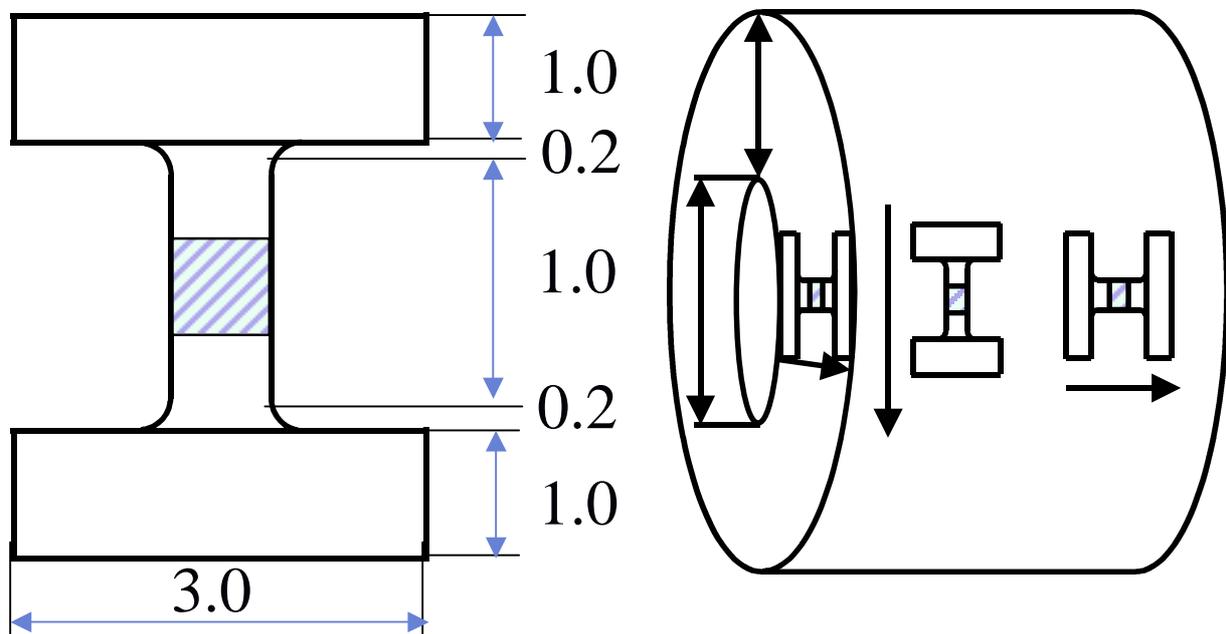


Fig. 4. The geometry of a small tensile specimen and a diagram of the machining in a pressure tube.

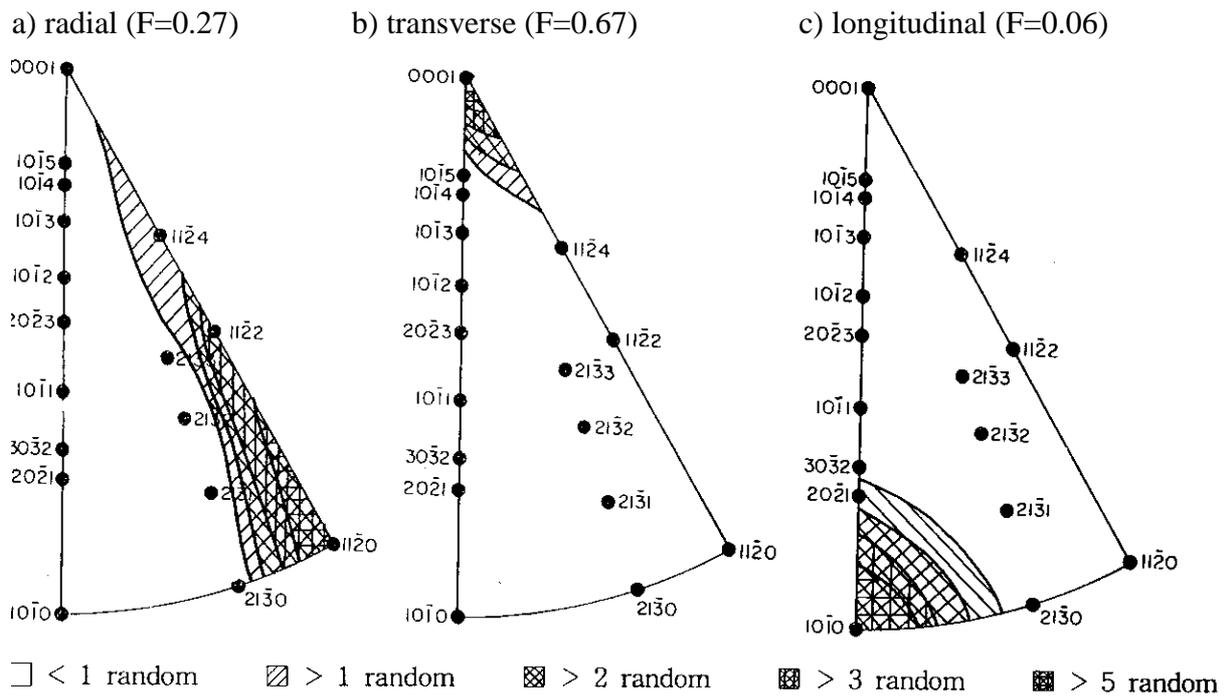


Fig. 5. Inverse pole figures for as-received Zr-2.5%Nb pressure tube material.

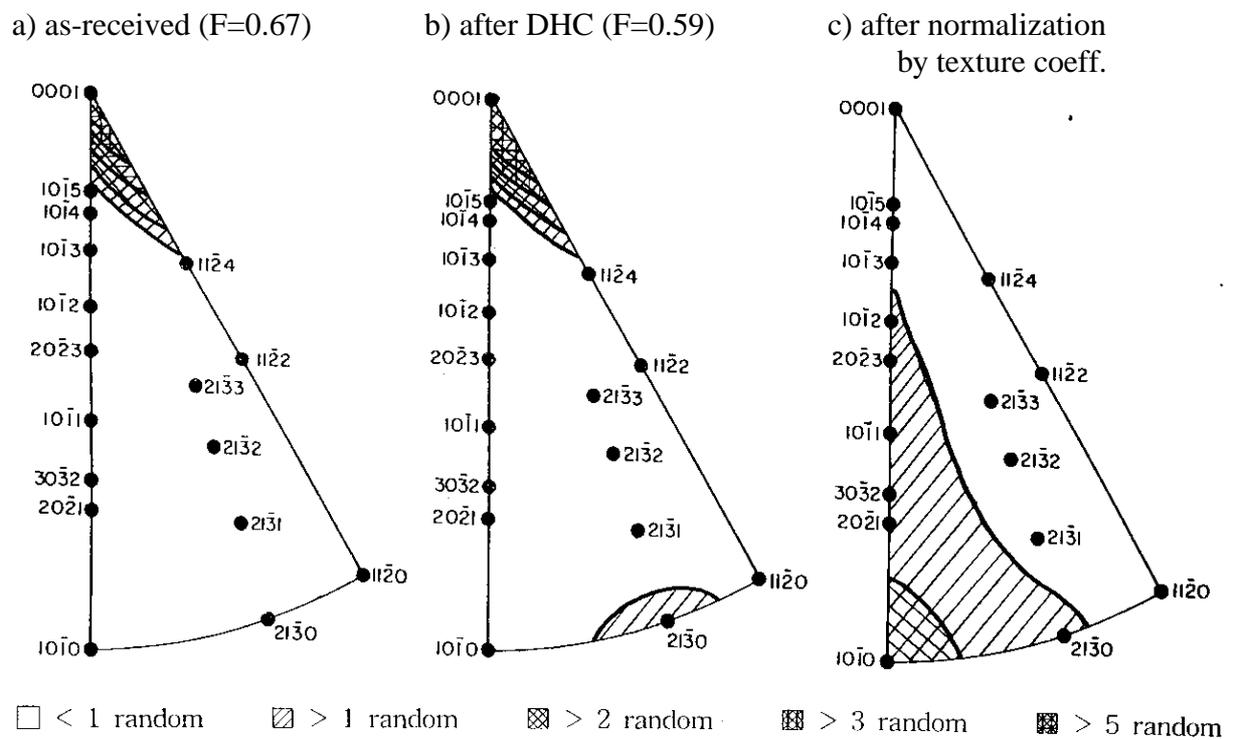


Fig. 6. Comparison of texture before and after DHC cracking in the longitudinal direction (CT).

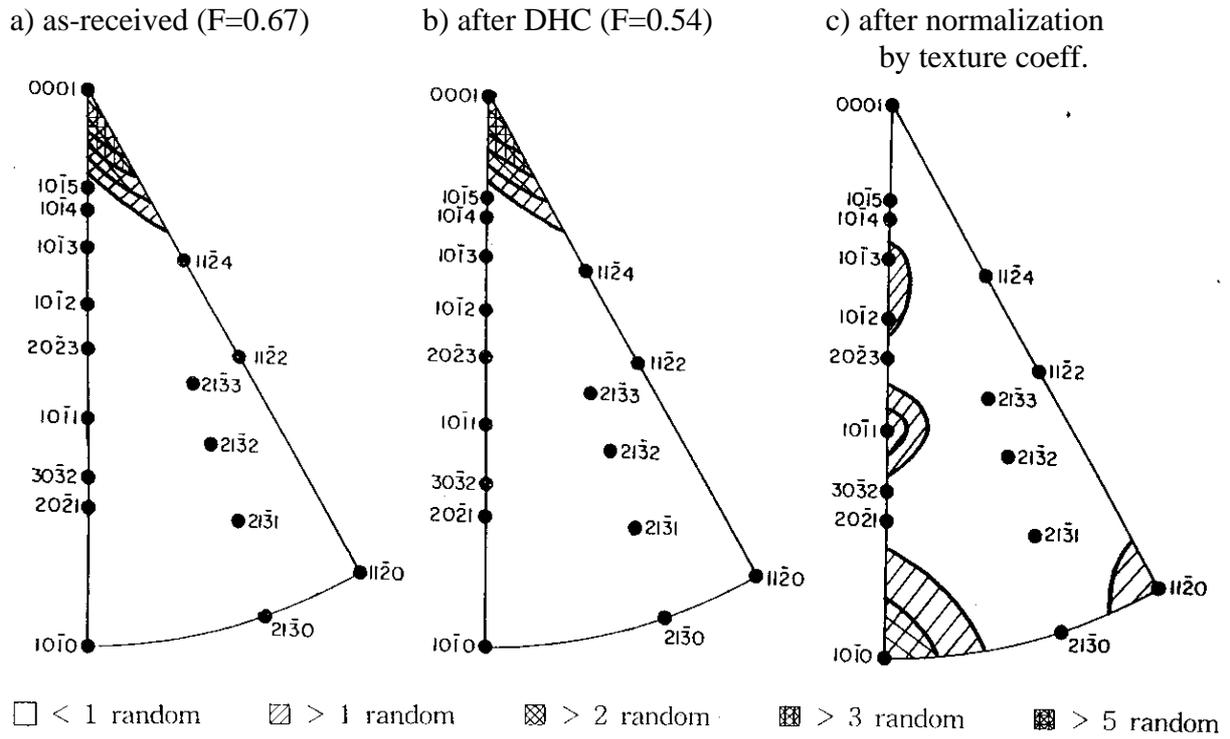


Fig. 7. Comparison of textures before and after DHC cracking in the radial direction (CB).

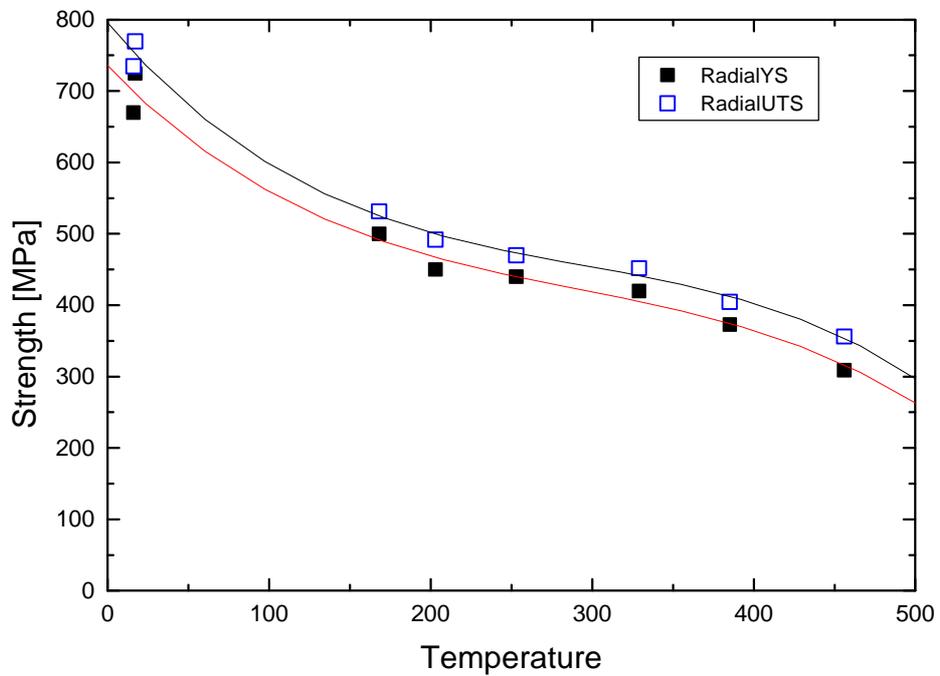


Fig. 8. Yield and tensile strengths measured from small tensile specimens in the radial direction.

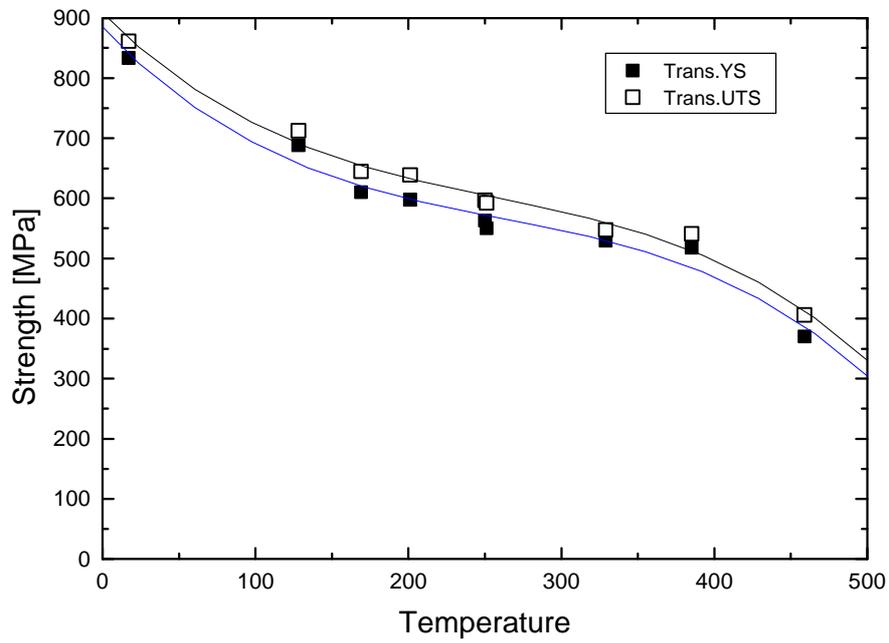


Fig. 9. Yield and tensile strengths measured from small tensile specimens in the transverse direction.

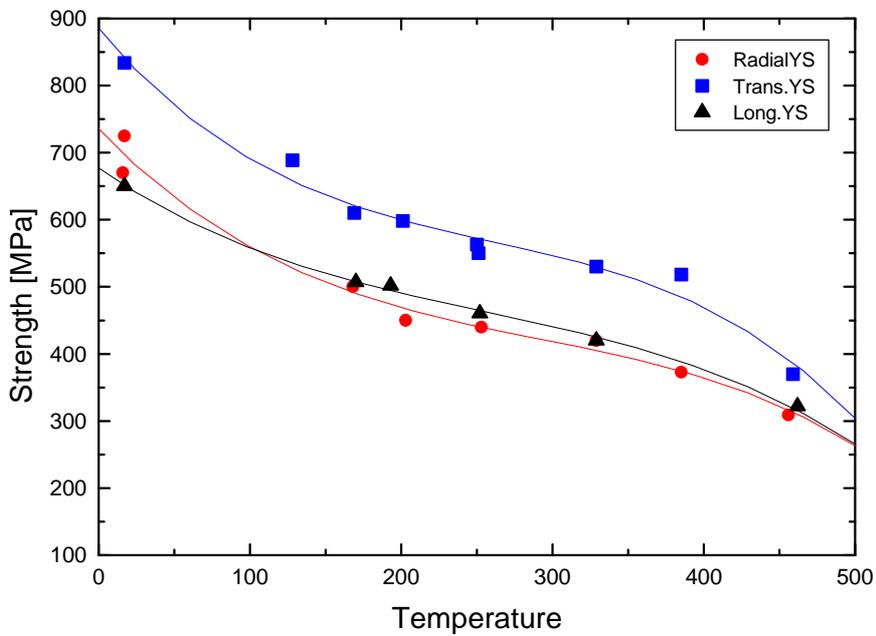


Fig. 10. Comparison of the yield strength in the radial, longitudinal, and transverse direction.

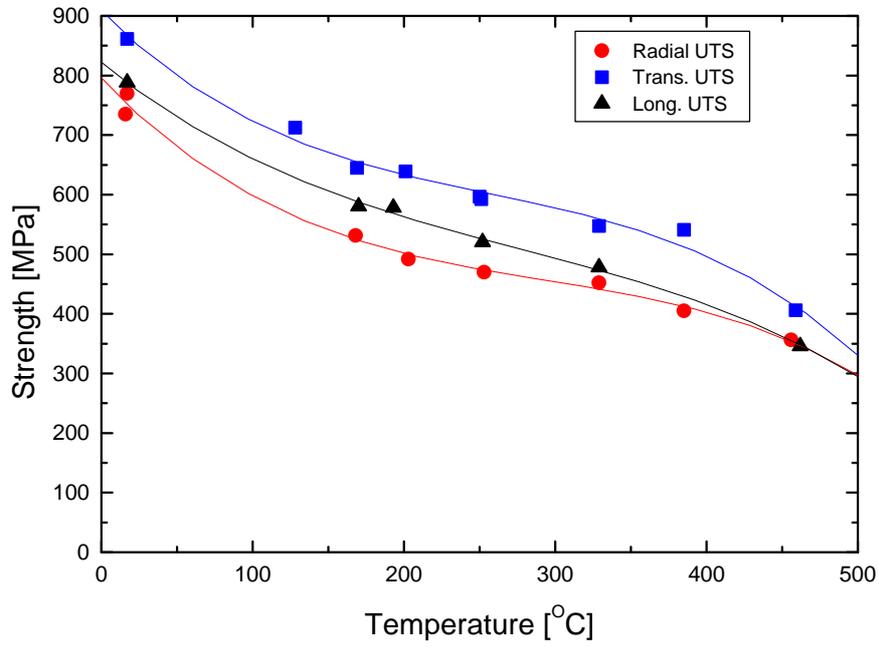


Fig. 11. Comparison of the tensile strength in the radial, longitudinal, and transverse direction.

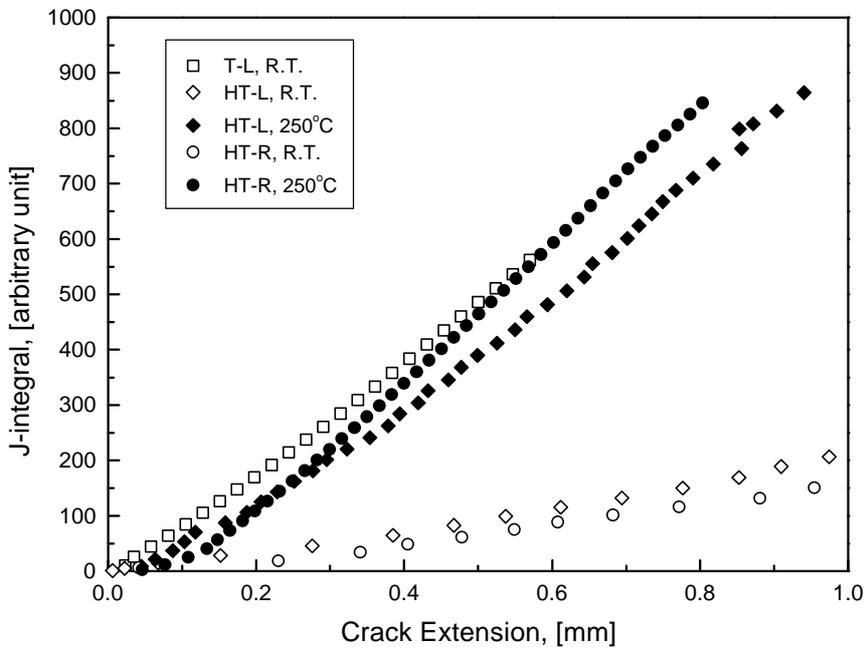


Fig. 12. J-integral and crack extension curves at RT and 250°C.